

Nonlinear Control for Magnetic Levitation of Automotive Engine Valves

Katherine Peterson, *Member, IEEE*, Jessy Grizzle, *Fellow, IEEE*,
and Anna Stefanopoulou, *Member, IEEE*

Abstract—Position regulation of a magnetic levitation device is achieved through a control Lyapunov function (CLF) feedback design. It is shown mathematically and experimentally that by selecting the CLF based on the solution to an algebraic Riccati equation it is possible to tune the performance of the controller using intuition from classical LQR control. The CLF is used with Sontag’s universal stabilizing feedback to enhance the region of attraction and improve the performance with respect to a linear controller. While the controller is designed for and implemented on an electromagnetic valve actuator for use in automotive engines, the control methodology presented here can be applied to generic magnetic levitation.

I. INTRODUCTION

Electromagnetic levitation is a classic control problem for which numerous solutions have been proposed. Many of the proposed solutions have focused on the use of feedback linearization [1], [3], [8]–[10], [15] due to the nonlinear characteristics of the magnetic and electric subsystems. Unfortunately, feedback linearization requires a very accurate model which may be unrealistic near the electromagnet due to magnetic saturation and eddy current effects, thereby limiting the range of motion achievable in the closed-loop system. Sliding mode [1], [2], [12] and H_∞ [14], [20] control have been used to

account for the changing local dynamics and to provide robustness against unmodeled nonlinearities present in the system. Linearization and switching can be avoided through the application of nonlinear control based on backstepping [5], [6] and passivity [18].

The control design investigated here is based on control Lyapunov functions (CLF) and Sontag’s universal stabilizing feedback [16]. The control Lyapunov function is selected based on a solution to an algebraic Riccati equation to allow us to “tune” the controller for performance. Neither current control nor a static relationship between current, voltage, and the magnetic force is assumed, as done by Velasco-Villa [18] and Green [6]. Instead, the dynamics of the current/flux are compensated for through the use of a full-state feedback/observer structure. Implementation is achieved using position and current sensors, a nonlinear observer to estimate velocity, a novel method to estimate the magnetic flux, and voltage control. To demonstrate the effectiveness of the controller, it is experimentally evaluated on an electromagnetic valve actuator designed for use in the actuation of automotive engine valves.

II. ELECTROMAGNETIC VALVE ACTUATOR

The electromagnetic valve actuator (EVA), shown in Fig. 1, has recently received attention due to its potential

Support is provided by NSF and Ford Motor Company.

to improve the performance of the standard internal combustion engine. Currently, valve motion in most automotive engines is controlled via a camshaft, which mechanically links the valve motion to the motion of the crankshaft. By de-coupling the valve motion from the crankshaft, the EVA allows for more flexibility in optimizing fuel economy, torque, and emissions [7]. In addition to providing variable valve timing (VVT), the EVA is capable of achieving variable valve lift (VVL) through magnetic levitation. With the exception of our previous work [11], research on the control of the EVA has primarily focused on the elimination of large impacts that occur between the armature and lower and upper magnetic coils. In this paper we expand on our previous work [11], which only briefly touched on the subject of magnetic levitation.

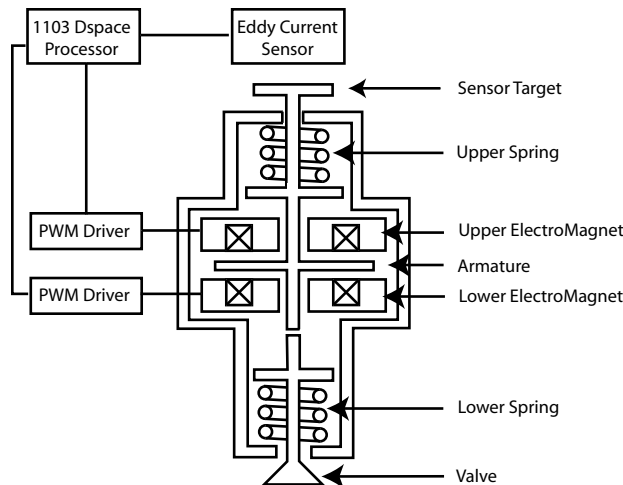


Fig. 1. Electromagnetic valve actuator and experimental setup.

The electromagnetic valve actuator governs the valve motion in the following manner. The armature is initially held against the upper magnetic coil, causing the valve to seal off the engine cylinder. In this position, the upper spring is more compressed than the lower spring creating

a force imbalance as the upper and lower springs are identical. When the valve open command is issued, the current in the upper magnetic coil is reduced to zero and the potential energy stored in the upper spring drives the armature downward, causing the valve to open. Depending on the command to the actuator, two outcomes are possible. In the case of full valve opening, the lower magnetic coil is used to bring the armature in contact with the lower electromagnet, and held there. From the view point of stability, this is the trivial case as the armature can be held against the lower magnetic coil by applying a sufficiently large constant voltage command. In the case of partial valve lift, the electromagnets are used to hover the armature. As the electromagnets can only apply attractive forces, the upper magnetic coil is used to hover the armature above the mid-position and the lower magnetic coil is used to hover the armature below the mid-position. When the valve closed command is issued, the upper magnetic coil and any potential energy stored in the lower spring are used to return the armature/valve to the closed position.

Hovering the armature is slightly different than the classic control problem of magnetic levitation due to the presence of the springs. When both electromagnets are de-energized, the armature sits at rest equidistant from either electromagnet. As shown by Tai [17], any equilibrium position that is greater than $1/3$ the full lift away from either electromagnet is open-loop exponentially stable. However, the presence of the springs does not necessarily make the control problem appreciably easier. As the springs are extremely stiff, the bandwidth of the mechanical subsystem is on the order of the bandwidth of the electrical subsystem. Therefore, it is not practical to assume current control as will be shown in Sec. VI. In addition, the region of attraction of the open-loop stable equilibria are small. It was found experimentally that

the armature had to start at rest equidistant from both electromagnets to achieve stable open-loop hovering for equilibrium positions greater than 1/3 the full lift away from either electromagnet. If the armature starts at rest against the upper magnetic coil, application of the open-loop equilibrium voltage results in the armature being brought into contact with the activated electromagnet. As the latter initial condition is the one experienced during operation, it is necessary to design a closed-loop controller to enlarge the region of attraction so that hovering is achieved for both open-loop stable and unstable equilibrium positions.

III. MODELING THE ELECTROMAGNETIC VALVE ACTUATOR

As derived by Wang [19] the dynamics of the EVA are given by

$$\begin{aligned}\frac{dz}{dt} &= v \cdot 10^3 \\ \frac{dv}{dt} &= \frac{1}{m} (F_{mag}^u - F_{mag}^l + k_s(l - z) - bv) \\ \frac{d\lambda_l}{dt} &= \left(V_l - \frac{r\lambda_l(k_b + z)}{k_a} \right) \cdot 10^3. \\ \frac{d\lambda_u}{dt} &= \left(V_u - \frac{r\lambda_u(k_b + 2l - z)}{k_a} \right) \cdot 10^3.\end{aligned}$$

where z (mm) is the distance from the lower coil, v (m/s) is the velocity of the armature, λ_l (mVs) is the magnetic flux in the lower coil, λ_u (mVs) is the magnetic flux in the upper coil, m (kg) is the combined mass of the armature and valve, F_{mag}^l (N) is the magnetic force generated by the lower coil, F_{mag}^u (N) is the magnetic force generated by the upper coil, k_s (N/mm) is the spring constant, l (mm) is half the total armature travel, b (kg/s) is the damping coefficient, V_l (V) is the voltage applied to the lower coil, V_u (V) is the voltage applied to the upper coil, and r (Ω) is the combined resistance

of the wiring and magnetic coil. Numerical values for all constants are found in Tab. I. Finally, the magnetic force generated by either coil is given by

$$F_{mag} = \frac{\lambda^2}{2k_a}. \quad (1)$$

As explained in Sec. II, only one electromagnet is used to hover the armature. Therefore, without loss of generality we assume that the lower coil is used and neglect the dynamics of the upper coil. To simplify the controller design, new inputs and coordinates are introduced per

$$\begin{aligned}x_1 &= z - z_{eq} \\ x_2 &= v - v_{eq} \\ x_3 &= \lambda_l - \lambda_{eq} \\ u &= V_l - V_{eq},\end{aligned}$$

where z_{eq} , v_{eq} , λ_{eq} , and V_{eq} are the equilibrium position, velocity, flux, and voltage respectively. The equilibrium point is now located at the origin, and the system dynamics are represented in the form

$$\frac{dx}{dt} = f(x) + g(x)u \quad (2)$$

where

$$\begin{aligned}f(x) &= \begin{bmatrix} x_2 \cdot 10^3 \\ \frac{1}{m} \left(-\frac{x_3^2}{2k_a} - k_s x_1 - b x_2 \right) - \frac{x_3 \lambda_{eq}}{k_a m} \\ - \left(\frac{x_3(k_b + z_{eq} + x_1)r}{k_a} + \frac{x_1 \lambda_{eq} r}{k_a} \right) \cdot 10^3 \end{bmatrix} \\ g(x) &= \begin{bmatrix} 0 & 0 & 10^3 \end{bmatrix}^T.\end{aligned}$$

A frequent assumption in the control of electromagnetic actuators is that the dynamics of the current/flux are significantly faster than the dynamics of the mechanical components of the system. This assumption reduces

the complexity of the control problem as most of the nonlinearities are present in the dynamics of current/flux. Unfortunately, this assumption is not valid for our system. The bandwidth of position is approximately equal to the bandwidth of current/flux due to the presence of stiff springs. To illustrate this phenomenon a comparison of the frequency response of flux and position is included in Fig. 2 for $z_{eq} = 2$ mm and a unity DC gain. The three different frequency response plots for position correspond to the nominal spring stiffness, the spring stiffness reduced by a factor of 10, and the spring stiffness reduced by a factor of 100. For the nominal spring stiffness, the bandwidth of both position and flux are approximately equal. As the spring stiffness is decreased, the bandwidth of flux remains approximately constant while the bandwidth of position is equal to the natural frequency of the mechanical subsystem,

$$\omega_n = \sqrt{\frac{k_s}{m}}. \quad (3)$$

Clearly, without the springs the bandwidth of the electrical/magnetic subsystem is significantly greater than the bandwidth of the mechanical subsystem. As no such bandwidth separation occurs in the nominal system, the controller design must therefore take the flux dynamics into account.

IV. EXPERIMENTAL SETUP

The experimental results which follow are conducted on the setup shown schematically in Fig. 1 and pictorially in Fig. 3. The position of the armature is determined from the eddy current sensor that detects changes in a self-generated magnetic field caused by the motion of the sensor target. The current in each coil is measured by built-in sensors in the PWM drivers. Based on these signals, the dSpace 1103 processor specifies the duty

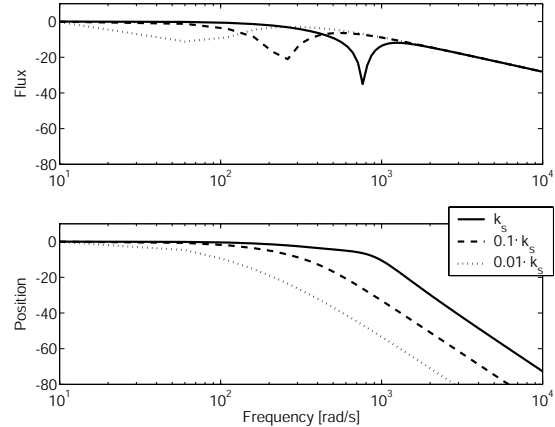


Fig. 2. Frequency response from Voltage to flux and position for different spring constants.

cycle to each PWM driver to control the motion of the armature. We assume that the PWM drivers are sufficiently fast that the applied voltage is equivalent to the commanded duty cycle multiplied by the supply voltage of 180 V.

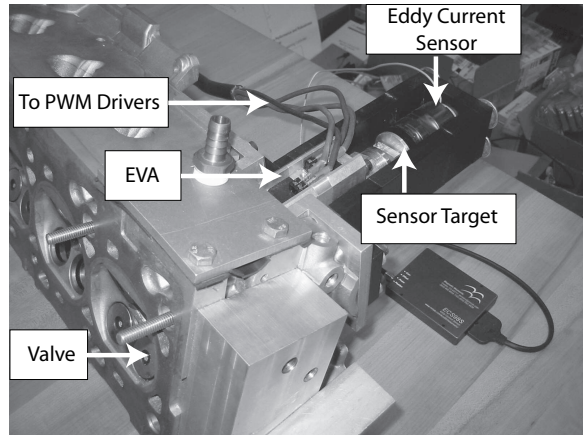


Fig. 3. Experimental Setup.

In the results that follow in Figs. 4, 5, 6, 7, 8, 10, and 11; the upper magnetic coil is located at $z = 8$ mm, the lower magnetic coil is located at $z = 0$ mm, the signal shown is the unfiltered position based on the

eddy current sensor mounted on the rear of the actuator, and the armature is released from rest against the upper magnetic coil at the beginning of the experiment unless otherwise specified.

V. OPEN LOOP CONTROL

As stated in Sec. II, Tai [17] has previously shown that the EVA is unstable for all equilibrium positions less than $2l/3$ mm away from either electromagnet. Based on how we have defined position, the system is open-loop exponentially stable in the range $2.6 \text{ mm} < z_{eq} < 5.3 \text{ mm}$. Despite being stable, it is difficult to achieve hovering in this range with open-loop control as the region of attraction is small. If the armature starts at rest against the upper magnetic coil (which is the normal mode of operation), application of the open-loop voltage for $z=2.6 \text{ mm}$ causes the armature to collide and remain in contact with the lower coil; see Fig. 4. To achieve stable open-loop hovering at $z=2.6 \text{ mm}$ the armature must start at rest equidistant from either magnetic coil ($z = 4 \text{ mm}$); see Fig. 4. As the latter condition is never experienced in operation, a closed-loop controller is needed to not only stabilize the unstable equilibria, but to also extend the region of attraction of the stable equilibria.

VI. CONTROLLER DESIGN

The proposed controller consists of two components, a stabilizing controller to achieve hovering and a damping controller that retards the initial motion of the armature during release. The stabilizing controller is based on Sontag's universal stabilizing feedback [16]. Two different control Lyapunov functions (CLF) for use with Sontag's feedback are given. While the first CLF is valid, the resulting performance achieved by it is poor. This motivates the selection of a new CLF based on the

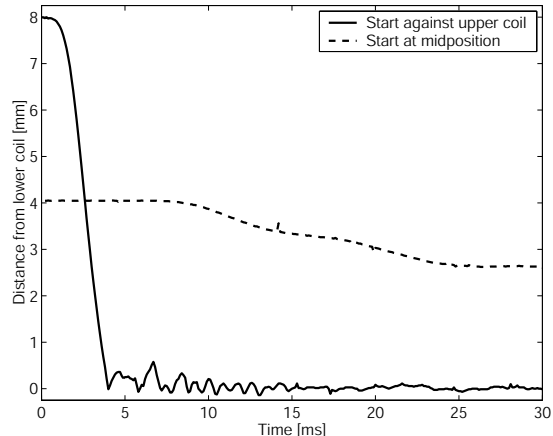


Fig. 4. Results of applying open-loop voltage for an equilibrium point 2.6 mm away from the lower coil.

solution to an algebraic Riccati equation. A mathematical proof and experimental results are given to show that selecting the CLF in this manner enables the designer to tune for performance. Since the electromagnet can only apply attractive forces, the upper coil is used to slow the release of the armature to reduce overshoot near the lower coil. The effects of actuator saturation are discussed later on in Sec. IX.

A. Stabilizing Controller

As the flux dynamics are non-negligible, see Sec. III, we have used Sontag's feedback [16] to stabilize the three state system. Given a Lyapunov function, V , such that

$$V \geq 0 \quad \forall x \in R^3 \quad (4)$$

$$V = 0 \quad \text{iff } x = 0, \quad (5)$$

it is said to be a Control Lyapunov function (CLF) if it satisfies the additional constraint

$$L_g V = 0 \quad \Rightarrow \quad L_f V < 0 \quad (6)$$

for all $x \neq 0$ such that $\|x\| < \delta$, where $L_f V$ and $L_g V$ are the Lie derivatives of the CLF, defined as

$$L_f V = \frac{\partial V}{\partial x} f(x) \quad (7)$$

$$L_g V = \frac{\partial V}{\partial x} g(x). \quad (8)$$

If the conditions given in Eqns. (4), (5), and (6) are satisfied, then Sontag's feedback given as

$$u = \begin{cases} -\frac{L_f V + \sqrt{L_f V^2 + (L_g V L_g V^T)^2}}{L_g V} & \text{for } L_g V \neq 0 \\ 0 & \text{for } L_g V = 0 \end{cases}$$

renders the origin asymptotically stable.

To implement Sontag's feedback, we propose the Lyapunov function

$$V = \begin{bmatrix} x_1 & x_2 \end{bmatrix} P_{nl} \begin{bmatrix} x_1 & x_2 \end{bmatrix}^T + \gamma x_3^2 \quad (9)$$

as a candidate CLF, where γ is constant and positive and the matrix P_{nl} satisfies the Lyapunov equation

$$A_{nl}^T P_{nl} + P_{nl} A_{nl} + Q_{nl} = 0, \quad (10)$$

where

$$A_{nl} = \begin{bmatrix} 0 & 10^3 \\ -k_s/m & -b/m \end{bmatrix} \text{ and} \\ Q_{nl} = \begin{bmatrix} q_1^2 & 0 \\ 0 & q_2^2 \end{bmatrix}.$$

Since A_{nl} is Hurwitz and Q_{nl} is positive definite, the matrix P_{nl} is positive definite. Solving for $L_g V$

$$L_g V = \begin{bmatrix} \frac{dV}{dx_1} & \frac{dV}{dx_2} & \frac{dV}{dx_3} \end{bmatrix} \begin{bmatrix} 0 & 0 & 10^3 \end{bmatrix}^T \quad (11)$$

$$L_g V = 2 \cdot 10^3 \gamma x_3 \quad (12)$$

Therefore

$$L_g V = 0 \quad \text{iff} \quad x_3 = 0. \quad (13)$$

When $x_3 = 0$, $L_f V$ is given as

$$L_f V = \left(\begin{bmatrix} \frac{dx_1}{dt} & \frac{dx_2}{dt} \end{bmatrix} P_{nl} \begin{bmatrix} x_1 & x_2 \end{bmatrix}^T + \begin{bmatrix} x_1 & x_2 \end{bmatrix} P_{nl} \begin{bmatrix} \frac{dx_1}{dt} & \frac{dx_2}{dt} \end{bmatrix}^T \right) \\ L_f V = \left(\begin{bmatrix} x_1 & x_2 \end{bmatrix} A_{nl}^T P_{nl} \begin{bmatrix} x_1 & x_2 \end{bmatrix}^T + \begin{bmatrix} x_1 & x_2 \end{bmatrix} P_{nl} A_{nl} \begin{bmatrix} x_1 & x_2 \end{bmatrix}^T \right) \\ L_f V = - \begin{bmatrix} x_1 & x_2 \end{bmatrix} Q_{nl} \begin{bmatrix} x_1 & x_2 \end{bmatrix}^T,$$

showing that Eqn. (9) is a Control Lyapunov function.

Formulating Sontag's feedback based on Eqn. (9) and implementing it on the experimental setup described in Sec. IV, we are able to achieve stable hovering as shown in Fig. 5. However, the performance is quite oscillatory. By adjusting q_1 , q_2 , and γ , it is possible to affect the performance, but it is not obvious how they should be manipulated to achieve the desired results. For this reason, a better candidate CLF is sought.

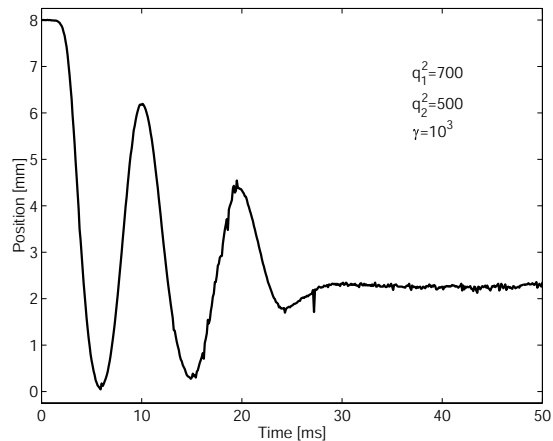


Fig. 5. Stable hovering achieved with the CLF given in Eqn. (9) on the experimental setup described in Sec. IV.

Let us instead select the CLF to be

$$V = x^T P x, \quad (14)$$

where the matrix P satisfies the algebraic Riccati equation

$$PA + A^T P + Q - PBB^T P = 0 \quad (15)$$

for

$$A = \left. \frac{\partial f(x)}{\partial x} \right|_{x=0} \quad (16)$$

$$B = g(x)|_{x=0}. \quad (17)$$

For convenience, the CLF given in Eqn. (14) will henceforth be referred to as the LQ-CLF. The motivation in selecting the CLF in this manner is that we can hopefully influence the performance of the system by manipulating the LQR cost function

$$J = \int_0^\infty (x^T Q x + u^2) dt \quad (18)$$

subject to the dynamics

$$\frac{dx}{dt} = Ax + Bu, \quad (19)$$

in order to select P . Note that even though we have chosen a quadratic Lyapunov function based on the linearized system model, the full nonlinear model is used when formulating Sontag's feedback. Selecting the CLF based on this method is not a new idea, and has previously been employed by Fontaine [4], although he does not use Sontag's feedback in conjunction with it.

Sepulchre [13] has shown that Sontag's feedback is optimal with respect to a given cost function. However for most systems the cost function is too complicated to give insight into the performance. Instead, let us restrict our view to what happens locally about equilibrium.

Near equilibrium, the Lie derivatives are approximated by

$$L_f V \approx 2x^T P A x = x^T (PA + A^T P) x \quad (20)$$

$$L_g V \approx 2x^T P B, \quad (21)$$

and thus Sontag's feedback is given as

$$u = - \frac{x^T (PA + A^T P) x}{2x^T P B} - \frac{\sqrt{(x^T (PA + A^T P) x)^2 + (4x^T P B B^T P x)^2}}{2x^T P B}.$$

From the Riccati inequality

$$x^T P B B^T P x > x^T (PA + A^T P) x, \quad (22)$$

therefore if x is sufficiently small

$$4(x^T P B B^T P x) \gg x^T (PA + A^T P) x \quad (23)$$

such that we can assume

$$u \approx - \frac{x^T (PA + A^T P) x + 4x^T P B B^T P x}{2x^T P B} \quad (24)$$

$$u \approx - \frac{4x^T P B B^T P x}{2x^T P B} \quad (25)$$

$$u \approx -2B^T P x. \quad (26)$$

Thus locally about the origin Sontag's feedback is approximately twice the LQR optimal feedback. Therefore we expect that the familiar process of tuning the LQR should be applicable for tuning Sontag's feedback. The effect of tuning the matrix Q from Eqn. (18) is seen in Fig. 6. The hovering point has been set to the mid-position and the matrix Q listed in Table II for $z_{eq} = 4$ is used. The $(2, 2)$ element of Q is varied according to the value given in each subplot. Manipulating the penalty on velocity significantly increases the effective closed-loop damping. It should be noted that the oscillations are

not caused by the controller, but rather the closed-loop response approaches the free response of the system as the (2, 2) element of Q is reduced.

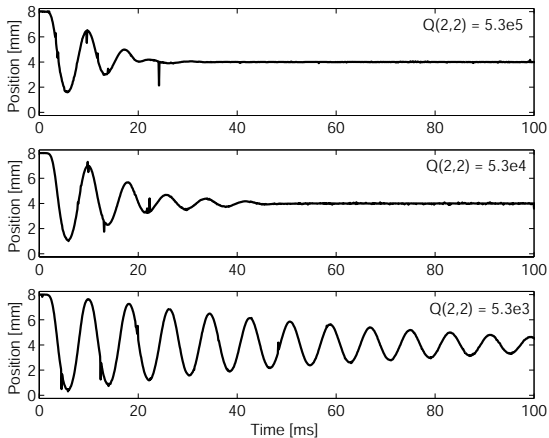


Fig. 6. Effects of tuning the matrix Q determined experimentally on the setup described in Sec. IV.

Based on this procedure, we can select an appropriate LQ-CLF and compare the results with those of Fig. 5; see Fig. 7. In Fig. 7, $z_{eq} = 2$ and the matrix Q is given in Table II. Using the LQ-CLF, we are able to dampen the response of the system and reduce the number of oscillations. Examining Fig. 7, the obvious question is: why wasn't the controller able to eliminate or at least reduce the initial overshoot? The answer is that the controller is unable to eliminate the initial overshoot due to the physical limitations of the actuator. When released from rest against the upper coil, the armature swings to within 0.5 mm of the lower coil due to the potential energy stored in the springs. As the electromagnet is only capable of applying attractive forces, the controller is unable to effect the initial overshoot. In Sec. VI-B, we explore how the releasing coil can be used to solve this problem.

Despite this problem, the LQ-CLF has several advantages that should not be overlooked. First, it is signif-

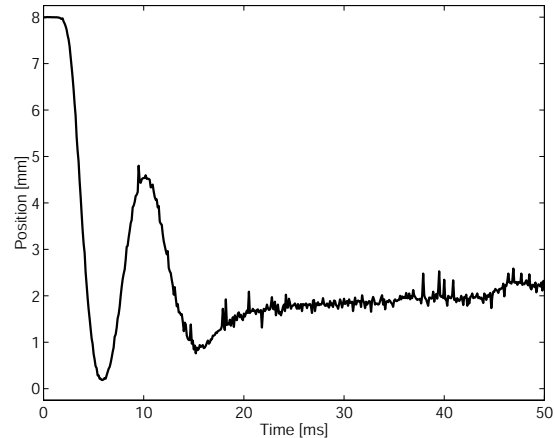


Fig. 7. Stable hovering achieved with the LQ-CLF on the experimental setup described in Sec. IV.

icantly easier to derive a CLF based on the algebraic Riccati equation than the one given in Eqn. (9). While the matrix P_{nl} is derived from a Lyapunov equation, structuring the Lyapunov function in the form given in Eqn. (9) requires insight into the dynamics of the system. In contrast, the LQ-CLF is formulated by simply linearizing the nonlinear system. Second, the LQ-CLF achieves better performance and the methodology for tuning is the same as the LQR, which is familiar to most control engineers. While it was somewhat possible to tune the performance with the original CLF, there is no clear methodology and it primarily involves trial.

B. Damping the Release

To remove the excess potential energy stored in the upper spring, and thus dampen the armature motion, the upper coil must be utilized as the electromagnets are only capable of applying attractive forces. One solution would be to select a multi-input CLF so that the feedback can utilize both magnetic coils. Unfortunately, it is not practical to select a multi-input CLF using the method explained in Sec. VI-A due to the dynamics of the EVA.

For equilibria below the mid-position, the effect of the upper coil on the motion of the armature is lost in the linearization. This is a result of the fact that the magnetic force is proportional to the square of the flux and the equilibrium flux in the upper coil is zero. Therefore the effect of the upper coil on the motion of the armature will not be utilized to minimize the penalty on position and velocity in Eqn. (18).

When hovering, the following methodology is used to dampen the release of the armature:

- 1) For both hovering above and below the mid-position, the voltage across the upper coil is set to -30 V until the armature has moved 0.1 mm away from the upper coil.
- 2) If the equilibrium position is at or above the mid-position, the closed-loop controller is activated after the armature has moved 0.1 mm away from the upper coil.
- 3) If the equilibrium position is below the mid-position, the voltage across the upper coil is set to 180 V until the armature is greater than 2 mm away from the upper coil. After this point, the voltage across the upper coil is set to zero and the closed-loop controller is activated. Once the estimated velocity reaches zero, the flux in the upper coil is driven to zero with the proportional controller

$$V_u = -5\lambda_u$$

since the armature has begun to move away from the lower coil and thus the upper coil can no longer effect the overshoot.

The effectiveness of this releasing methodology is shown in Fig. 8. As with Fig. 7, $z_{eq} = 2$ mm and the matrix Q is given in Table II.

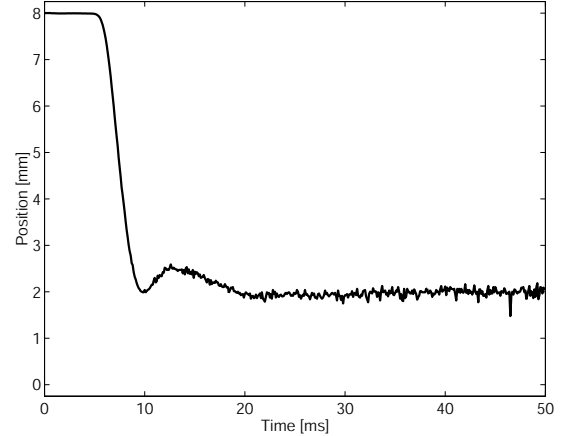


Fig. 8. Stable hovering achieved with the LQ-CLF and dampened release on the experimental setup described in Sec. IV.

VII. NONLINEAR OBSERVER

As the actuator is intended for use in an automotive engine it is impractical to measure every state. The available measurements are the position of the armature and the current in each coil. Current is chosen over flux as current sensors are standard in most power electronic devices and the compact design of the actuator prevents the mounting of hall effect sensors.

First, the magnetic flux is determined using a map of the magnetic force as a function of current and position developed by Wang [19], denoted as $F_{mag}(i, z)$. Given the position and current, the magnetic flux is determined by

$$\lambda = \sqrt{2k_a F_{mag}(i, z)}, \quad (27)$$

based on Eqn (1). Second, the armature velocity is estimated by the nonlinear observer

$$\begin{aligned} \frac{d\hat{z}}{dt} &= \hat{v} + \Gamma_1(z, \hat{z}) \\ \frac{d\hat{v}}{dt} &= \frac{1}{m}(k_s(l - \hat{z}) - b\hat{v}) + \Gamma_2(i_l, i_u, z, \hat{z}), \end{aligned}$$

where

$$\Gamma_1(z, \hat{z}) = g_1(z - \hat{z})$$

$$\Gamma_2(i_u, i_u, z, \hat{z}) = F_{mag}^u(i_u, z) - F_{mag}^l(i_l, z) + g_2(z - \hat{z})$$

Computing the error dynamics, $e = \begin{bmatrix} z - \hat{z} \\ v - \hat{v} \end{bmatrix}$, results in

$$\frac{de}{dt} = \underbrace{\begin{bmatrix} 0 & 1000 \\ -k_s/m & -b/m \end{bmatrix}}_{A_r} e + \begin{bmatrix} g_1 \\ g_2 \end{bmatrix} \underbrace{\begin{bmatrix} 1 & 0 \end{bmatrix}}_{C_r} e$$

where the pair (A_r, C_r) is observable. Values for the output injection gains g_1 and g_2 are given in Table. I. Convergence of the estimated velocity is shown in Fig. 9.

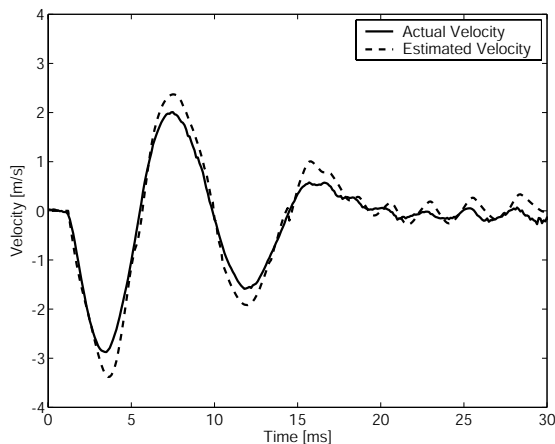


Fig. 9. Comparison of the actual vs. estimated velocity.

In its final form, the controller is implemented using the measured position, the estimated velocity from the observer, and the approximated flux using Eqn. (27) based on the measured position and current.

VIII. EXPERIMENTAL RESULTS

The overall performance of the controller is presented in Figs. 10 and 11, which show the armature hovering at

several different equilibrium positions. The Q matrices used in conjunction with Eqn. (18) to select the CLFs for each equilibrium point are given in Table. II. Recall from Sec. V that all equilibrium points less $1/3$ the total lift (approximately 2.6 mm) away from either electromagnet are open-loop unstable. As shown in Fig. 10, we are able to hover the armature approximately 1 mm away from either electromagnet. In addition to stabilizing the unstable equilibrium points, the region of attraction of the stable equilibrium points ($2.6 \text{ mm} < z < 5.3 \text{ mm}$) has been improved such that stable hovering is achieved when the armature is released from rest against the upper magnetic coil. Recall from Sec. V that this was problematic with open-loop control.

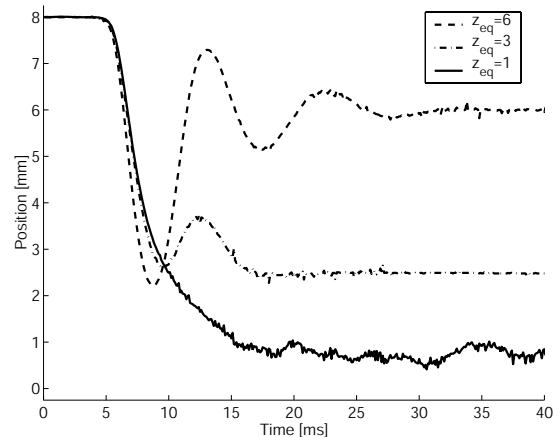


Fig. 10. Armature hovering at 1 mm, 3 mm, and 6 mm away from the lower coil achieved on the experimental setup described in Sec. IV.

IX. LINEAR VS. NONLINEAR CONTROL

Having shown in Sec. VI-A that locally Sontag's feedback approximates the Linear Quadratic Regulator, is there an advantage to using Sontag's feedback instead of its linear approximation? To answer this question let us examine the nonlinear terms lost during linearization.

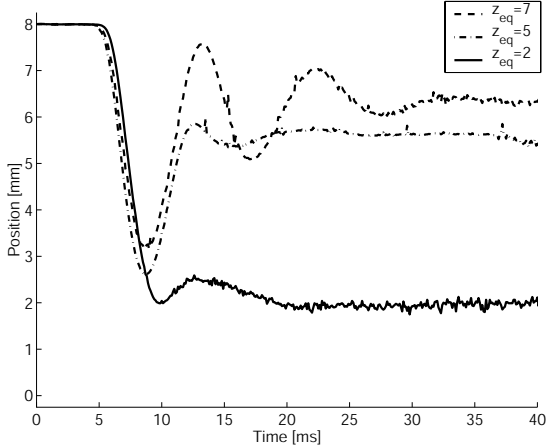


Fig. 11. Armature hovering at 2 mm, 5 mm, and 7 mm away from the lower coil achieved on the experimental setup described in Sec. IV.

The state space representation given in Eqn. (2) can be expressed as

$$\frac{dx}{dt} = Ax + \Delta f(x) + Bu$$

where the matrices A and B are given by

$$A = \begin{bmatrix} 0 & 1 & 0 \\ -\frac{k_s}{m} & -\frac{b}{m} & -\frac{\lambda_{eq}}{2k_a m} \\ -\frac{r\lambda_{eq}}{2k_a} & 0 & -\frac{r(k_b + z_{eq})}{2k_a} \end{bmatrix},$$

$$B = \begin{bmatrix} 0 & 0 & 1 \end{bmatrix}^T,$$

and

$$\Delta f(x) = \begin{bmatrix} 0 & \frac{-x_3^2}{2k_a m} & -\frac{x_3 x_1 r}{k_a} \cdot 10^3 \end{bmatrix}^T. \quad (28)$$

Therefore the difference between the nonlinear and linear model, and thus to some extent Sontag's feedback and its linear approximation, given in Eqn. (26), are the terms contained in $\Delta f(x)$. The term

$$-\frac{x_3 x_1 r}{k_a} \cdot 10^3 \quad (29)$$

which affects the dynamics of x_3 , is stabilizing if $x_1 > 0$, which occurs for $z > z_{eq}$. As the inequality $z > z_{eq}$ is valid for the majority of the armature travel, the loss of the nonlinear term of Eqn. (29) should not have a detrimental impact on the performance of the linear approximation of Sontag's feedback. The effect of the 2^{nd} term

$$\frac{-x_3^2}{2k_a m} \quad (30)$$

is not as benign. Due to the loss of this term, the linear model (and thus the linear approximation) underestimates the attractive force generated by the magnetic coil. Thus we expect the linear approximation to experience more overshoot than Sontag's feedback as the magnitude of the nonlinear term in Eqn. (30) increases. Minimizing overshoot is an important consideration since excessive overshoot may lead to impacts between the armature and electromagnets.

Through simulation of both Sontag's feedback and its linear approximation, see Eqn. (26), a better understanding of the difference can be gained in the absence of noise and other variations that occur from one experiment to the next. Comparisons of the simulated response of Sontag's feedback and its linear approximation are given in Figs. 12, 13, 14, and 15 for several different equilibria. The controller used to dampen the release of the armature has been turned off to avoid obscuring the results.

As stated previously, we expect to observe more overshoot in the linear approximation of Sontag's feedback as the nonlinear term in Eqn. (30) increases. Recall that

$$x_3 = \lambda_l - \lambda_{eq}.$$

Since λ_{eq} increases as z_{eq} decreases, the effect should be more prevalent for equilibrium positions near the

electromagnet. In addition, the effects should be more noticeable at the beginning of the transition as λ_l is initially zero and thus x_3 is large. These trends can both be observed in Figs. 12 and 13, which show that the linear approximation of Sontag’s feedback experiences more overshoot. In the case of hovering 0.5 mm away from the electromagnet, Fig. 13, this results in an impact between the armature and the magnetic coil at approximately 5 ms into the transition. The increase in the overshoot observed in Figs. 12, and 13 is caused by the application of larger voltages during the initial part of the transition. As mentioned before, this is expected as x_3 takes on its largest value at the beginning of the transition when $\lambda_l = 0$. Later in the transition the voltage specified by the linear approximation tends to dip below Sontag’s feedback in an attempt to compensate for the increased overshoot.

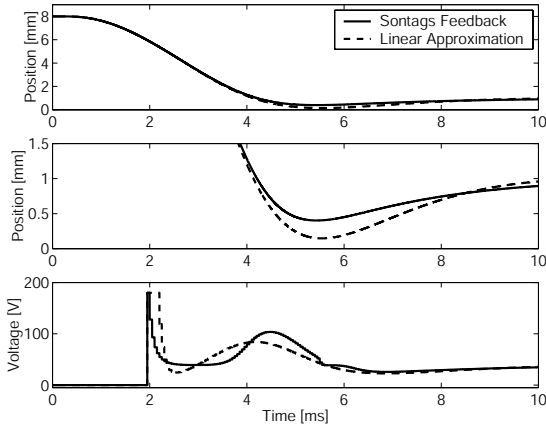


Fig. 12. Simulated response of the armature hovering 1 mm away from the magnetic coil.

For equilibrium positions further away from the lower magnetic coil, the performance of both Sontag’s feedback and its linear approximation appear to be more similar; see Figs. 14 and 15. Upon closer examination, the applied voltage determined by each controller is very

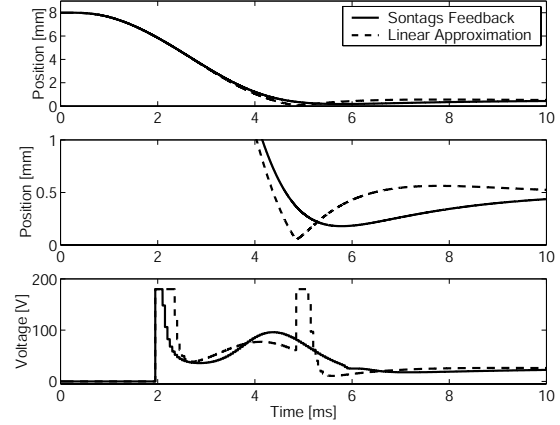


Fig. 13. Simulated response of the armature hovering 0.5 mm away from the magnetic coil.

different despite that the position trace is quite similar. To understanding why this difference arises let us take a brief aside to discuss actuator saturation.

As mentioned in Sec. IV, the power supply can provide a maximum voltage of 180 V. Since the PWM drivers can reverse the polarity of the applied voltage, the controller can therefore potentially apply voltages in the range of -180 V to 180 V. However this creates a potential problem. If the controller is allowed to apply negative voltages, it may attempt to “push” on the armature by generating negative flux in the magnetic coil. Since the magnetic force is proportional to the square of the magnetic flux, Eqn. (1), the application of negative magnetic flux generates an attractive force, thus creating a potentially unstable feedback loop.

To avoid this, the following saturation logic is used;

$$V_l = \begin{cases} 180 & \text{if } V_l^{fb} > 180 \\ V_l^{fb} & \text{if } 0 \leq V_l^{fb} \leq 180 \\ V_l^{fb} & \text{if } -180 \leq V_l^{fb} \leq 0 \text{ and } \lambda_l \geq 5 \\ 0 & \text{if } V_l^{fb} \leq 0 \text{ and } \lambda_l < 5 \end{cases} \quad (31)$$

where V_l^{fb} is the voltage specified by the feedback.

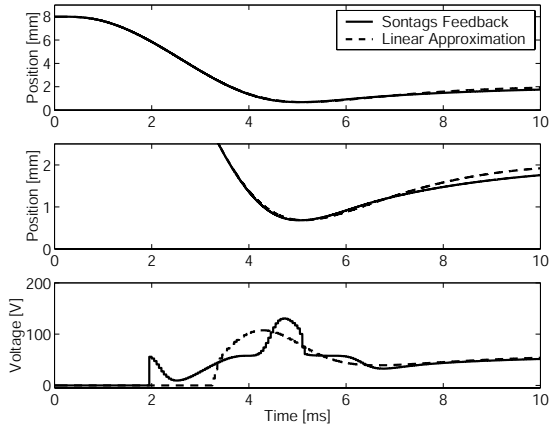


Fig. 14. Simulated response of the armature hovering 2 mm away from the magnetic coil.

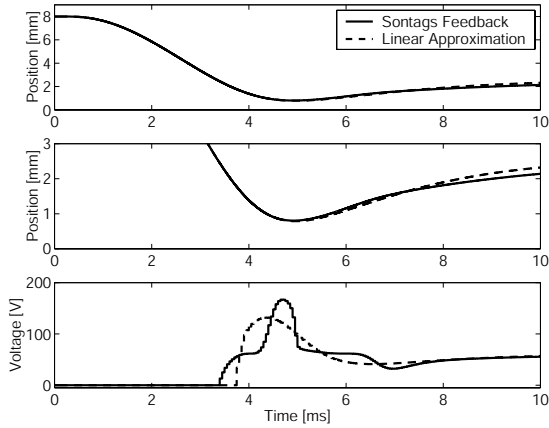


Fig. 15. Simulated response of the armature hovering 2.5 mm away from the magnetic coil.

This allows the controller to apply negative voltages in order to reduce the flux if need be, but not to generate negative flux. The effects of removing this logic is shown in Figs. 16 and 17. In the case of hovering 2 mm away from the lower coil, the linear approximation of Sontag’s feedback initially applies a negative voltage in an attempt to “push” on the armature. In the case of hovering 2.5 mm away from the lower coil, both Sontag’s feedback and the linear approximation apply a

negative voltage during the initial part of the transition, however the linear approximation generates larger values of negative magnetic flux. Again, the linear approximation tends to attempt to “push” on the armature more frequently due to the loss of the nonlinear term given in Eqn. (30). Despite that this is avoided by using the saturation logic given in Eqn. (31), the use of Sontag’s feedback is advantageous as it is more likely to apply a meaningful control input as shown in Figs. 14 and 15 by the fact that it becomes non-zero sooner.

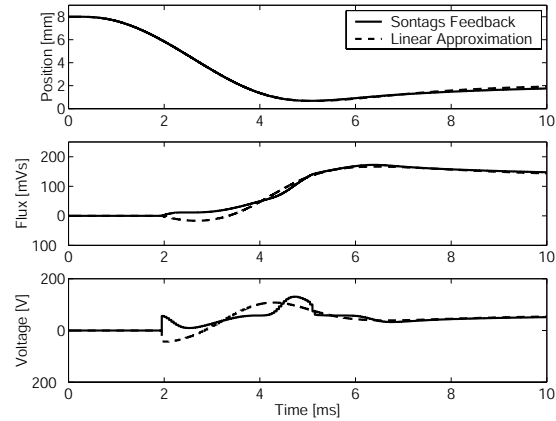


Fig. 16. Simulated response of the armature hovering 2 mm away from the magnetic coil without the saturation logic given in Eqn. (31).

X. CONCLUSION

Stable hovering is achieved for a wide range of lift conditions for an electromagnetic valve actuator using Sontag’s feedback. It was shown mathematically and experimentally that by selecting the CLF based on the solution to the algebraic Riccati equation, it is possible to tune the performance of the controller using the familiar LQR procedure. Future work will explore augmenting the controller with an integrator to eliminate the steady state tracking errors seen in Figs. 10 and 11 of Sec. VIII.

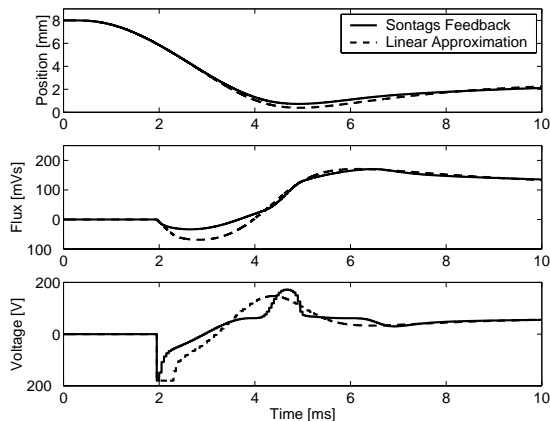


Fig. 17. Simulated response of the armature hovering 2.5 mm away from the magnetic coil without the saturation logic given in Eqn. (31).

TABLE I

NUMERICAL VALUES OF CONSTANTS.

Parameter	Numerical value	Parameter	Numerical value
m	0.27	k_b	0.04
k_s	158	q_1^2	700
l	4.0	q_2^2	500
b	7.53	γ	10^{-3}
r	6.0	g_1	3560
k_a	29.92	g_2	4820

REFERENCES

- [1] A. Charara, J. DeMiras, and B. Caron, "Nonlinear control of a magnetic levitation system without premagnetization," *IEEE Transactions on Control System Technology*, vol. 4, no. 5, pp. 513–523, Sept. 1996.
- [2] D. Cho, Y. Kato, and D. Spilman, "Sliding mode and classical control of magnetic levitation systems," *IEEE Control Systems*, pp. 42–48, Feb. 1993.
- [3] B. Fabien, "Observer-based feedback linearization control of an electromagnetic suspension," *ASME Journal of Dynamic Systems, Measurement and Control*, vol. 118, pp. 615–619, Sept. 1996.
- [4] D. Fontaine, S. Liao, J. Paduano, and P. Kokotovic, "Nonlinear control experiments on an axial fbw compressor," *Conference on Decision and Control*, pp. 1329–1334, December 2000.
- [5] L. Gentili and L. Marconi, "Robust nonlinear disturbance sup-

TABLE II

NUMERICAL VALUE OF THE MATRIX Q.

Numerical value of Q	For
diag [1, 4.7e4, 10]	$z_{eq} = 1.0$ and $z_{eq} = 7.0$
diag [1, 6.6e4, 10]	$z_{eq} = 2.0$ and $z_{eq} = 6.0$
diag [1, 1.2e5, 10]	$z_{eq} = 3.0$ and $z_{eq} = 5.0$
diag [1, 5.3e5, 10]	$z_{eq} = 4.0$

pression of a magnetic levitation system," *Automatica*, vol. 39, no. 4, pp. 735–742, April. 2003.

- [6] S. Green and K. Craig, "Robust, digital nonlinear control of magnetic-levitation systems," *ASME Journal of Dynamic Systems, Measurement and Control*, vol. 120, no. 4, pp. 488–495, Dec. 1998.
- [7] M. Levin and M. Schechter, "Camless engine," *SAE 960581*, 1996.
- [8] J. Lindlau and C. Knospe, "Feedback linearization of active magnetic bearing with voltage control," *IEEE Transactions on Control Systems Technology*, vol. 10, no. 1, January 2002.
- [9] L. Mao and J. Li, "Feedback linearisation of magnetic bearing actuators for a uniform upper bound of force slew rate," *IEE-Proceedings-Electric-Power-Applications*, vol. 146, no. 6, July 1999.
- [10] C. Munaro, M. Filho, R. Borges, S. Munareto, and W. DaCosta, "Modeling and observer-based nonlinear control of a magnetic levitation system," *IEEE Conference on Control Applications - Proceedings*, vol. 1, pp. 162–167, 2002.
- [11] K. Peterson and A. Stefanopoulou, "Rendering the electromechanical valve actuator globally asymptotically stable," *Proc. IEEE Conference on Decision and Control*, pp. 1753–1758, Dec. 2003.
- [12] A. Rundell, S. Drakunov, and R. DeCarlo, "A sliding mode observer and controller for stabilization of rotational motion of a vertical shaft magnetic bearing," *IEEE Transactions on Control Systems Technology*, vol. 4, no. 5, pp. 598–608, Sept. 1996.
- [13] R. Sepulchre, M. Jankovic, and P. Kokotovic, *Constructive Nonlinear Control*. Springer, 1997.
- [14] K. Shibukawa, T. Tsubakiji, and H. Kimura, "Robust stabilization of a magnetic levitation system," *Proceedings of the 30th IEEE Conference on Decision and Control*, vol. 3, pp. 2368–2371, 1991.
- [15] R. Smith and W. Weldon, "Nonlinear control of a rigid rotor magnetic bearing system: Modeling and simulation with full state

- feedback,” *IEEE Transactions on Magnetics*, vol. 31, no. 2, 1995.
- [16] E. Sontag, “A universal construction of artstein’s theorem on nonlinear stabilization,” *Systems and Control Letters*, vol. 13, no. 2, pp. 117–123, 1989.
- [17] C. Tai and T. Tsao, “Control of an electromechanical camless valve actuator,” *Proceedings American Control Conference*, May 2002.
- [18] M. Velasco-Villa, R. Castro-Linares, and L. Corona-Ramirez, “Modeling and passivity based control of a magnetic levitation system,” *IEEE Conference on Control Applications*, pp. 64–69, 2001.
- [19] Y. Wang, “Camless engine valvetrain: Enabling technology and control techniques,” Ph.D. dissertation, University of California Santa Barbara, 2001.
- [20] J. Yi, K. Park, S. Kim, Y. Kwak, M. Abdelfatah, and I. Busch-Vishniac, “Force control of magnetic levitation system using flux density measurement,” *Proceedings of the 34th IEEE Conference on Decision and Control*, vol. 3, pp. 2153–2158, 1995.